GEOPHYSICS, VOL. 80, NO. 3 (MAY-JUNE 2015); P. E197–E212, 17 FIGS., 2 TABLES.
10.1190/GEO2014-0381.1

And the geophysicist replied: "Which model do you want?"

Steven Constable[1], Arnold Orange[1], and Kerry Key[1]

ABSTRACT

Marine controlled-source electromagnetic (CSEM) and magnetotelluric (MT) soundings were carried out between 1997 and 2003 over the Gemini prospect in the Gulf of Mexico during early development of marine instrumentation. The resulting data sets provide a good test bed for examining the effect of the data type and misfit choice on regularized inversion solutions. We inverted the data sets individually and jointly for isotropic and anisotropic resistivity at a variety of data misfits. We found that multifrequency CSEM inversions vastly improved structural resolution over single-frequency inversions, suggesting that variation in skin depth added significant information. Joint MT and CSEM inversion appeared to improve resolution over MT-only inversions at depths considerably deeper than the CSEM data can resolve, probably by constraining shallow structure in the parts of the model to which the MT data were sensitive. The addition of model anisotropy improved data fit, but introduced an arbitrary scaling between the regularization penalty on model roughness and the penalty on anisotropy. A small relative penalty on anisotropy produced two independent models for horizontal and vertical resistivity, whereas a large penalty reproduced the isotropic models. Intermediate penalties produced pleasing models, but there was no objective criterion to choose one particular model. Inverted models also depend significantly on the choice of target data misfit, but the optimum misfit is difficult to determine even with well-estimated errors. So-called L-curves do not provide an objective choice of misfit because they are both heuristic and depend on the choice of data that is plotted. Various measures of structure in data residuals were tested in an attempt to guide the misfit choice, with some success, but this too was somewhat heuristic. Ultimately, of the 100 or so inversions that were run, no single model could be considered "preferred," but together they provided a good understanding of the information contained in the data.

INTRODUCTION

Passive and active source electromagnetic (EM) soundings, and in particular the magnetotelluric (MT) and controlled-source EM (CSEM) methods, are important tools for academic studies of earth's geologic processes and also for commercial resource exploration (recent reviews are given by Key, 2012a; Selway, 2014; Smith, 2014). The data generated from these methods, which are complex electric and magnetic fields and/or transfer functions between field components, do not lend themselves to direct interpretation, but they require comparison with a numerically generated synthetic response using a mathematic representation of an earth model. It has become common practice to use automated routines to generate models that are compatible with field observations. These routines may be statistically based, whereby many models are generated from some quasi-random process and are compared with the observed data, or deterministic, in which gradients derived from the forward model process and misfit surfaces are used to update a sequence of models which may, or may not, converge to a solution.

For higher dimensional models (2D and 3D), the size of the model space and the computational cost of the forward calculations generally preclude the use of statistical methods. Deterministic inverse methods are seductive in their simplicity, at least when they converge and achieve a good fit to the data: Feed them a data set and a starting model, and they return a model that fits the data. However, the widespread and effective use of higher dimensional inversion algorithms can inure the user to the underlying problems of geophysical inversion. The solutions are nonunique, and so if any solution can be found, there are an infinite number of other acceptable

Manuscript received by the Editor 14 August 2014; revised manuscript received 18 December 2014; published online 28 April 2015.
[1]Scripps Institution of Oceanography, La Jolla, California, USA. E-mail: sconstable@ucsd.edu; aorange@ucsd.edu; kkey@ucsd.edu.

solutions to be had. The solutions are also unstable, which means that very large changes to the model result in only small or even no change in the fit to the data. In mathematic parlance, the problem is ill posed.

Most deterministic methods require that some penalty be applied to the model to deal with instability and nonuniqueness. This may take a variety of forms, but almost every extant algorithm uses some variation on first derivative smoothness to stabilize the models, although other penalties can, and sometimes are, applied. A consequence of using similar smoothness penalties is that the models produced by the various inversion algorithms often look very similar for a given data set, providing some confidence that the results are meaningful. The results might well be meaningful, but the purpose of this paper is to highlight how models produced by even a single inversion algorithm can vary significantly depending on the selection of data and choice of misfit level. Many readers will be generally aware of this problem already, but we also demonstrate that for CSEM and MT data collected at multiple frequencies, inverted models can change in unexpected ways because different subsets of data are inverted individually or in combination.

Similar exercises to ours have been done before (e.g., Commer and Newman, 2009) but usually on synthetically generated data. Synthetic model studies are useful because the true models are known, and so the data distribution and the inversion algorithms can be tested for their ability to recover the known structure. However, synthetic models are unrepresentative of the real world in two ways: (1) The error statistics are well behaved and are known exactly. We make the case below that it is important to understand the error structure of the field data, but unfortunately, one can only go so far in estimating errors of real data, and they are rarely perfectly behaved. We show that differences in misfit that are smaller than the uncertainty in the error estimation produce significant differences in inverted models. (2) With few exceptions, the models used in synthetic studies are chosen to be simple structures within a homogenous host. In the real world, the host geology is not simple, and it may be variably anisotropic. Although the data may be sensitive to the presence of anisotropy, we show that it is difficult to quantify just how much anisotropy is present in the real earth structure from EM data alone.

We are particularly interested in the behavior of marine EM methods, although the conclusions we draw from this study apply to terrestrial data as well. Although a great deal of marine EM data is being collected, most of it is proprietary and collected over hydrocarbon reservoir targets, which do not generate a response in MT data. Recently developed CSEM processing tools (Myer et al., 2011) and inversion code (Key, 2012b) prompted us to return to a joint CSEM/MT data set collected more than a decade ago over the Gemini salt body in the Gulf of Mexico. These data are some of the earliest collected using the current generation of marine EM instruments. Indeed, the transmitter and most of the receivers used were prototypes in the development of the more mature systems described by Constable (2013). However, in spite of their age, these data are of reasonable quality and present a useful test bed for inversion because (a) they are publishable, (b) the data have been processed by the authors from raw time series using publicly available codes that (c) generate fairly reliable error bars, and (d) they have MT and CSEM responses available. Furthermore, the Gemini salt body structure is generally known from drilling and seismic studies.

INVERSION ALGORITHM

The inversion scheme we use in this study is the Occam algorithm of Constable et al. (1987). The Occam algorithm is one implementation of a regularized inversion approach (often called *Tikhonov regularization* [Tikhonov and Arsenin, 1977]) that has almost become ubiquitous in practical geophysical inversion, in which a cost function U formed from a weighted sum of data misfit and model penalty is minimized:

$$U = \|\mathbf{Wd} - \mathbf{W}f(\mathbf{m})\|^2 + \lambda\|\mathbf{Rm}\|^2, \tag{1}$$

where $\mathbf{W}$ is a weighting matrix of reciprocal data errors acting on the data vector $\mathbf{d}$ and the prediction of the forward functional $f(\mathbf{m})$ at model vector $\mathbf{m}$. The first term is thus a sum-square misfit, which will be χ^2 distributed for well-estimated, zero-mean, independent, and normally distributed data errors. The second term is the regularization on the model, where $\mathbf{R}$ extracts some penalty on the model, usually roughness through a first derivative process, although a variety of penalties can be used to achieve models with other characteristics, such as closeness to a prior model or models with a minimum number of sharp boundaries. The weighting or trade-off parameter λ balances the penalty between fitting the data and smoothing the model, and it also acts to stabilize the inversion; for $\lambda = 0$, the nonlinear least-squares solution that remains is usually underdetermined (i.e., there are more model parameters than independent data) and extremely unstable (linearized solutions will rapidly diverge).

Because the forward functional $f(\mathbf{m})$ is nonlinear for the EM sounding methods discussed below, equation 1 is usually solved iteratively by linearization around a starting model $\mathbf{m}_0$:

$$U = \|\mathbf{Wd} - \mathbf{W}(f(\mathbf{m}_0) + \mathbf{J}(\mathbf{m}_1 - \mathbf{m}_0))\|^2 + \lambda\|\mathbf{Rm}_1\|^2, \tag{2}$$

where $\mathbf{J}$ is the Jacobian matrix of partial derivatives of each datum with respect to each model parameter:

$$J_{ij} = \frac{\partial f(\mathbf{x_i}, \mathbf{m})}{\partial m_j}. \tag{3}$$

We have introduced $\mathbf{x_i}$ to represent the dependent variables describing the characteristics of the ith datum (frequency, position, complex component, etc.). The elements of $\mathbf{J}$ can be computed analytically, by differencing, or by an adjoint process. Equation 2 can then be solved for a model update $\Delta\mathbf{m} = \mathbf{m}_1 - \mathbf{m}_0$.

The scalar λ is essentially a free parameter, but it is one that has a profound effect on the model produced by minimizing equation 1. For a small λ, the model becomes very rough to achieve a small data misfit. For a large λ, the model becomes very smooth at the expense of fitting the data. One can carry out multiple inversions to explore the trade-off between misfit and roughness, but this can be computationally expensive and perhaps even prohibitively expensive for some 3D inversions of EM data, although some algorithms successively decrease λ as part of the inversion process. Often in practice, λ is chosen in a somewhat ad hoc manner based on experience. For example, Newman and Alumbaugh (1997) extract λ from statistics derived from the weighted Jacobian based on "extensive numerical experiments," and Commer and Newman (2008) set λ equal to a constant, which one suspects is by far the most common approach. It is also a common practice to include a penalty against the distance

from the starting model or a preferred model as well as a roughness penalty (e.g., Zhdanov et al., 2000), although this introduces a subjective bias in the resulting models.

Even though to some extent the term "Occam's inversion" has become synonymous with regularized inversion, probably because the 1987 paper was the first published practical application of regularization to nonlinear geophysical problems and was accompanied by public-domain computer code (Constable et al., 1987), it is in fact only one implementation of the general regularization method described above. Three aspects of this algorithm differentiate it from other methods.

First, rather than minimize over the data misfit, the Occam algorithm includes a target misfit χ^2_*:

$$U = (\|\mathbf{Wd} - \mathbf{W}f(\mathbf{m}_1)\|^2 - \chi^2_*) + \lambda\|\mathbf{Rm_1}\|^2. \quad (4)$$

The philosophy behind this is that with well-estimated data errors, a fairly objective estimate of reasonable data fit can be made based on the statistics of the chi-squared distribution, such as the expectation value or the 95% confidence value (although for large data sets, the difference between these is small). One practical aspect of introducing χ^2_* is that the data misfit is not implicitly dependent on an initial choice of λ, but it is explicitly dependent on the choice of χ^2_*. Another aspect is that if χ^2_* can be achieved by the inversion process, the misfit term goes to zero and the algorithm can converge to a solution that minimizes model roughness. Of course, there is no guarantee that the minimum is a global, rather than a local, minimum, and there is a lot of flexibility in how roughness is quantified (that is, how $\mathbf{R}$ is constructed), but experience suggests that because the Occam algorithm does not regularize against the starting model, if the starting model is simple (a half-space, for example), then the solution does not usually depend on the value of the starting model.

Second, rather than solving equation 2 for $\Delta\mathbf{m}$, the Occam algorithm solves for the next model in the iterative series:

$$\mathbf{m}_1 = [\lambda\mathbf{R}^T\mathbf{R} + (\mathbf{WJ})^T\mathbf{WJ}]^{-1}(\mathbf{WJ})^T\mathbf{W}(\mathbf{d} - f(\mathbf{m_0}) + \mathbf{Jm}_0). \quad (5)$$

This algorithm takes large steps through model space, aggressively reducing the misfit, which reduces the number of iterations required to converge on a solution. This is desirable because for nonlinear Newton-type algorithms, a new $\mathbf{J}$ needs to be computed at each iteration, a computationally expensive process for higher dimensional models. It can be seen from equation 5 why the regularization term stabilizes the solution; for 1D models, $\mathbf{R}$ is bidiagonal, and it improves the condition of the matrix inversion.

Third, the distinguishing feature of the Occam algorithm is the method for choosing λ. Instead of choosing λ arbitrarily or by some derived statistic, it is obtained by a 1D optimization of χ^2 versus λ at each iteration, using a mechanism such as a golden section search. Before the target misfit is achieved, λ is optimized to reduce the misfit as much as possible from the last iteration (phase 1). Once the target misfit is achieved, λ is optimized to produce the smoothest model (that is, to minimize the model penalty term), and if all goes well, the iterative process will converge and $\Delta\mathbf{m}$ will go to zero (phase 2) (see Constable et al. [1987] for details). These optimizations typically cost 5–10 matrix inversions and forward calculations at each iteration, but combined with solving directly for $\mathbf{m}_{i+1}$ greatly reduces the number of iterations required to reach a solution (to of order 10 for typical 2D MT problems). Importantly, the final model depends on the choice of χ^2_* rather than a choice of λ.

Figure 1 presents a cartoon of this behavior for a two-parameter problem. The figure illustrates that a small efficiency might be achieved by making a less abrupt transition from phase 1 to phase 2, but the more important point is that the algorithm needs to be run to convergence, and not just to the target misfit. A common mistake in the use of the algorithm is a failure to let the algorithm converge after the target misfit is obtained, which will result in models that are not maximally smooth for a given misfit.

In the next sections, we will apply the Occam algorithm repeatedly to a set of marine EM data collected in the Gulf of Mexico, to explore the dependencies of the model on data type and target misfit. The implementation of the inversion algorithm that we use is described in Key (2012b). This computer code uses a 2D unstructured finite-element mesh with adaptive refinement to ensure the accuracy of the forward calculations and is configured for CSEM and MT data. It allows anisotropy in the principal model directions and uses a parallelized architecture to speed execution time on multicore computers or clusters. All inversions presented in this paper were carried out on an eight-core Macintosh desktop having a processor speed of 2.93 GHz.

MT DATA COLLECTION AND PROCESSING

MT data were collected over the Gemini prospect in 1997, 1998, 2001, and 2003, during campaigns to develop the marine MT instrument described in Constable et al. (1998). Details of the data collection and processing are given in Key et al. (2006); for this work,

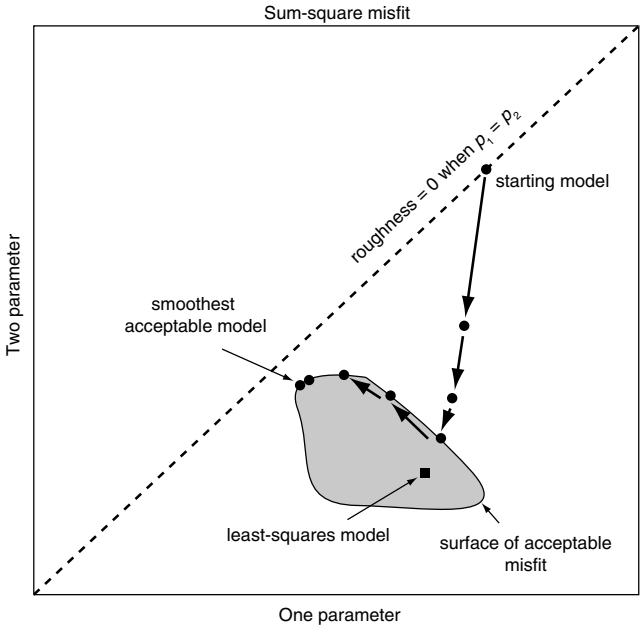

Figure 1. Diagrammatic representation of the Occam algorithm's path though model space, reduced to a sum-squared misfit for a two-parameter problem. Initial iterations reduce the sum-squared misfit χ^2 until the acceptable misfit χ^2_* is reached. The algorithm then reduces the roughness in the model until it converges on the smoothest model that fits the data to χ^2_*. The diagonal broken line represents the set of maximally smooth models.

we are using data collected on "line A" described in that paper. Deployments were typically of about two days' duration, and the data quality varied considerably depending on the state of instrument development and geomagnetic activity. The data were processed using the multistation transfer function estimation code of Egbert (1997).

The Gemini salt body is a complex, 3D structure, but the line of stations we use here is perpendicular to a fairly 2D northwest–southeast-trending ridge in the top-salt surface (Figure 2). An interpretation of seismic reflectivity shows a deep (7000 m) root in the salt to the northwest of line A, but a 3D inversion of the entire MT data set by Zhdanov et al. (2011) shows little evidence of resistive salt below approximately 5000 m, suggesting that MT data are not particularly sensitive to this feature (or that the seismic interpretation is not correct). The data are largely 1D in appearance with little separation between modes, but Key et al. (2006) show that 2D inversion did a good job of recovering structure as long as the mode with electric field perpendicular to the top-salt ridge was used. We follow their example to use only data that they called "inline electric" and inverted these as the transverse magnetic mode of the 2D MT nomenclature. These data are shown in Figure 3; there are 169 apparent resistivity and phase pairs distributed across 16 stations. The data were truncated at 3000-s periods to reduce sensitivity to large-scale 3D structures associated with bathymetry and coastlines.

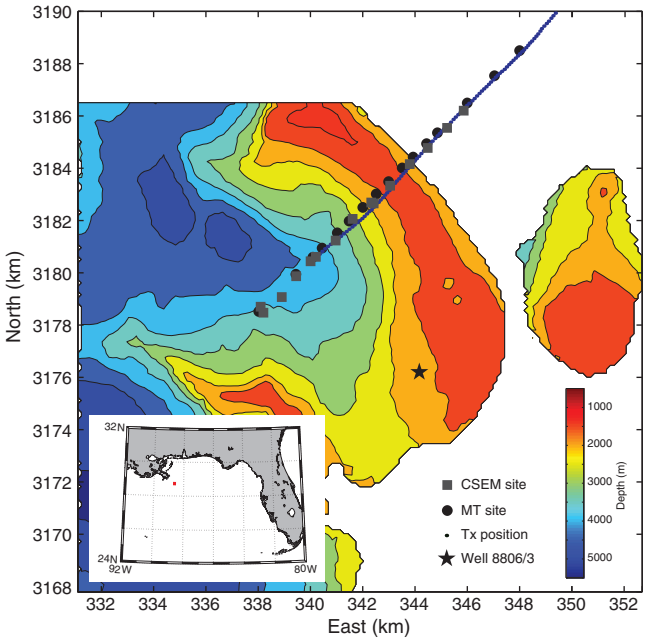

Figure 2. Locations of MT sites, CSEM receiver sites, transmitter sites, and well 8806/3 overlain on the top-salt depth (the salt geometry is courtesy of Chevron). The red square in the inset shows the location of the prospect in the Gulf of Mexico.

An important aspect of data processing is error estimation; inversion algorithms weight all data by their errors, so it is easy to see that the data error is equally as important as the actual data value. It has been shown that the algorithm of Egbert (1997) generates error estimates that are reasonably consistent with the variance from repeat sampling of marine MT data (Sherman et al., 2013), although we apply an error floor of 5% in resistivity and 1.45° in phase in recognition of the limitations in the forward model complexity. The maximum error in the MT apparent resistivities is 29%, and the mean is 6%. The maximum error in the phase is 8.3°, and the mean is 1.7°.

CSEM DATA COLLECTION AND PROCESSING

The marine CSEM data presented here were collected in January 2003 from the R/V *Gyre*. Fifteen receiver instruments were deployed along line A of the MT array, three configured as MT instruments with magnetometers, and twelve as instruments collecting electric field data only. The sampling rate was 31.25 Hz. All instruments were the Mk II version described by Constable (2013), fitted with 24-bit analog-to-digital converters. Receiver navigation after deployment was carried out using long-baseline acoustic ranging from the vessel. The prototype recording compasses that were used for instrument orientation did not perform particularly well, and so instrument orientations were estimated from the morphology of the MT and CSEM data.

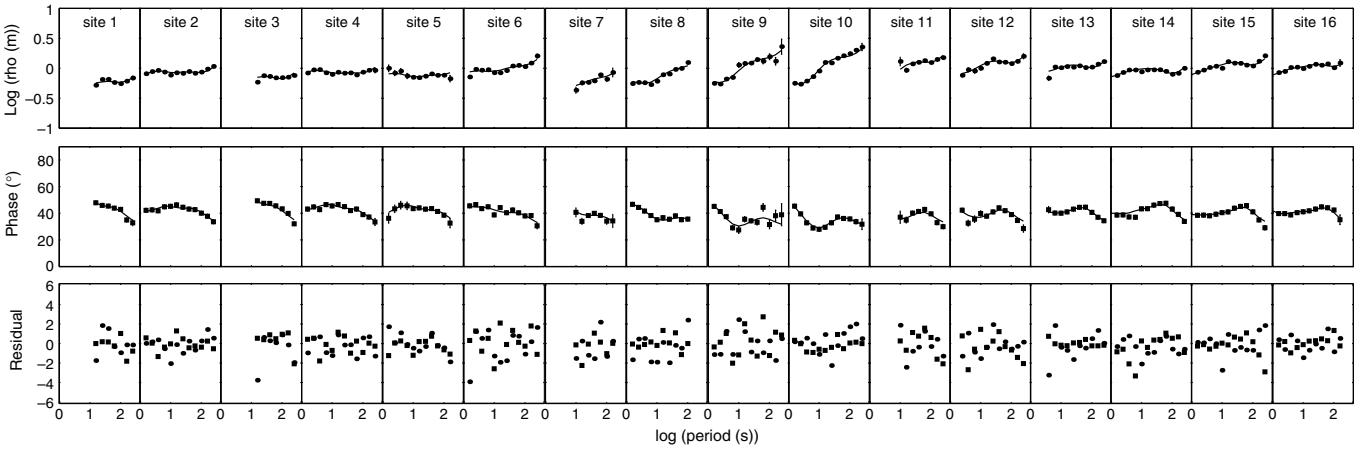

Figure 3. Marine MT data used in this project as a function of the site number. The model response and normalized residuals are from an anisotropic inversion fitting the entire CSEM and MT data set to an rms of 0.90, shown in Figure 12. The rms misfit for this data subset is 0.996.

This experiment was the first test of a prototype 200-A Scripps Undersea Electromagnetic Source Instrument. This system consists of a topside 30-kW power supply that transmits 2000 V, 400-Hz power down a coaxial, 17-mm cable to an instrument that is towed about 100 m above the seafloor. This deep-towed instrument transforms the high voltage to low voltage, rectifies it, and switches the polarity at relatively low frequency for transmission into the seawater through a 50–300-m antenna. Further details are given in Constable (2013). In this case, the transmitter was fitted with a 150-m, neutrally buoyant antenna cable and navigation was accomplished using a Kongsberg-Simrad ultrashort-baseline (USBL) acoustic system, with a standard acoustic head and motion reference unit mounted in the ship's well and tilted backward 20°. The vessel did not have an installed deep tow winch, and so, a 17-mm coaxial deep-tow cable and winch was rented for the project. Because this was the first use of the transmitter, we operate at half of the 2000 VAC maximum cable voltage, providing a zero to peak output current of 95 A. The waveform was the "Cox" waveform described in Constable and Cox (1996) and Myer et al. (2011), with a nominal fundamental frequency of 0.25 Hz. This waveform generates first, third, and seventh harmonics with amplitudes of 0.788, −0.788, and −0.208 times peak current. Unfortunately, we had not yet implemented GPS-stabilized power frequency control, and so, the frequency of the 400-Hz power was controlled by the internal oscillator of the topside power unit. The power supply oscillator drifted by approximately nine parts per thousand and was sufficiently unstable around this value that useful phase data could not be recovered from the receiver instruments. The data described below are thus only electric field amplitudes. We had intended to carry out several passes over the line of instruments, increasing transmission current and changing frequency, but during the turn at the end of the first pass, the rented winch freewheeled and dropped the transmitter and tow cable to the seafloor. These were recovered by dragging using a trawl cable guided by the USBL navigation, but the system was no longer suitable for continued work on this experiment afterward.

The data were processed using the algorithm of Myer et al. (2011), dividing the time series into 4-s windows (one cycle of the transmitted fundamental frequency) for Fourier transformation and averaging 30 of these windows to provide data sampled every 120 s. (A phase correction was applied to ensure that the transmitter phase drift did not corrupt the synchronous stacking.) There are several advantages to this approach, the most important being that the standard error in the mean can be computed for every individual data point. This not only provides objective error estimates, but it tracks any nonstationarity in environmental and instrumental noise. However, an error floor of 4% was applied to capture uncertainties in calibration, navigation, and the model approximations, and data with errors greater than 40% were excluded. Data at the three frequencies are shown in Figures 4–6. The average errors at 0.25, 0.75, and 1.75 Hz are 11.6%, 14.7%, and 22.7%, respectively.

INDIVIDUAL MT AND CSEM INVERSIONS

As a first test of the data error estimation and validity of the 2D approximation, we inverted each data subset (MT and each CSEM frequency) using an isotropic inversion starting at a 1-Ωm half-

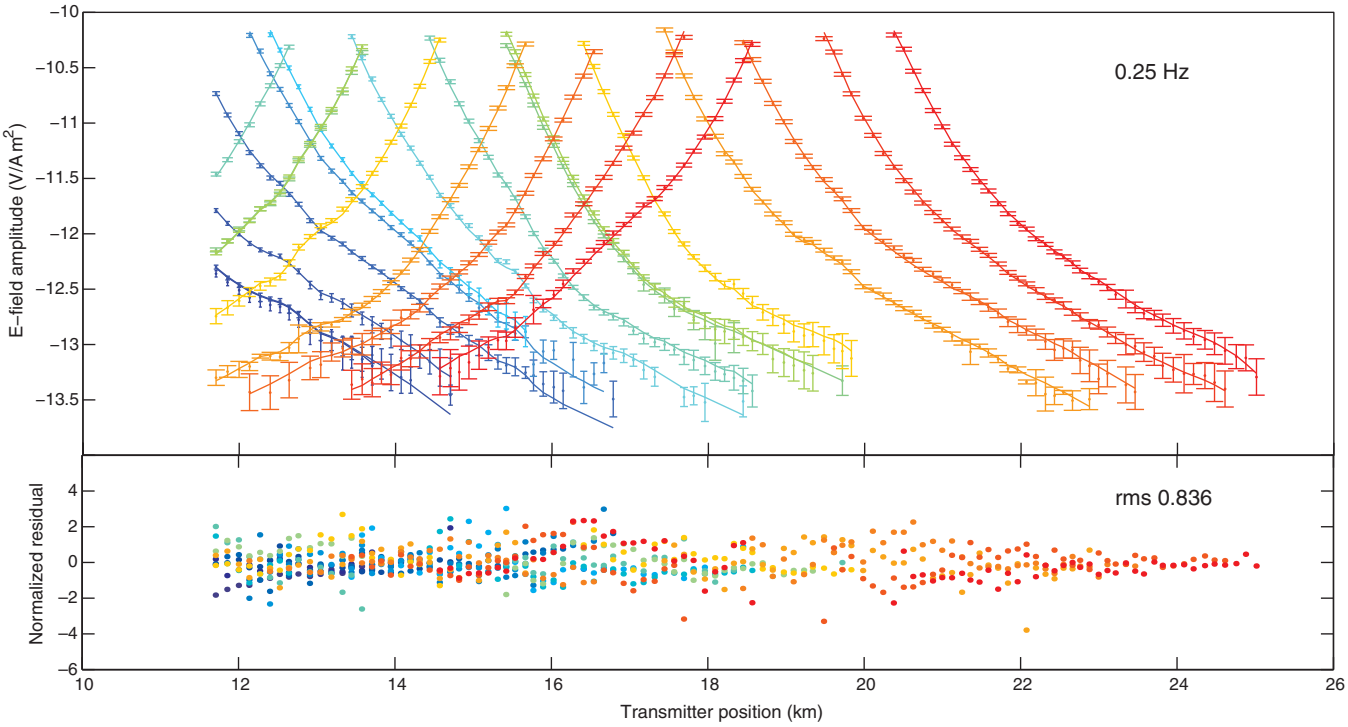

Figure 4. Marine CSEM data at the fundamental frequency of 0.25 Hz as a function of the transmitter position. The model response and normalized residuals are from an anisotropic inversion fitting the entire CSEM and MT data set to rms 0.90 and shown in Figure 12. The rms misfit for this data subset is 0.836.

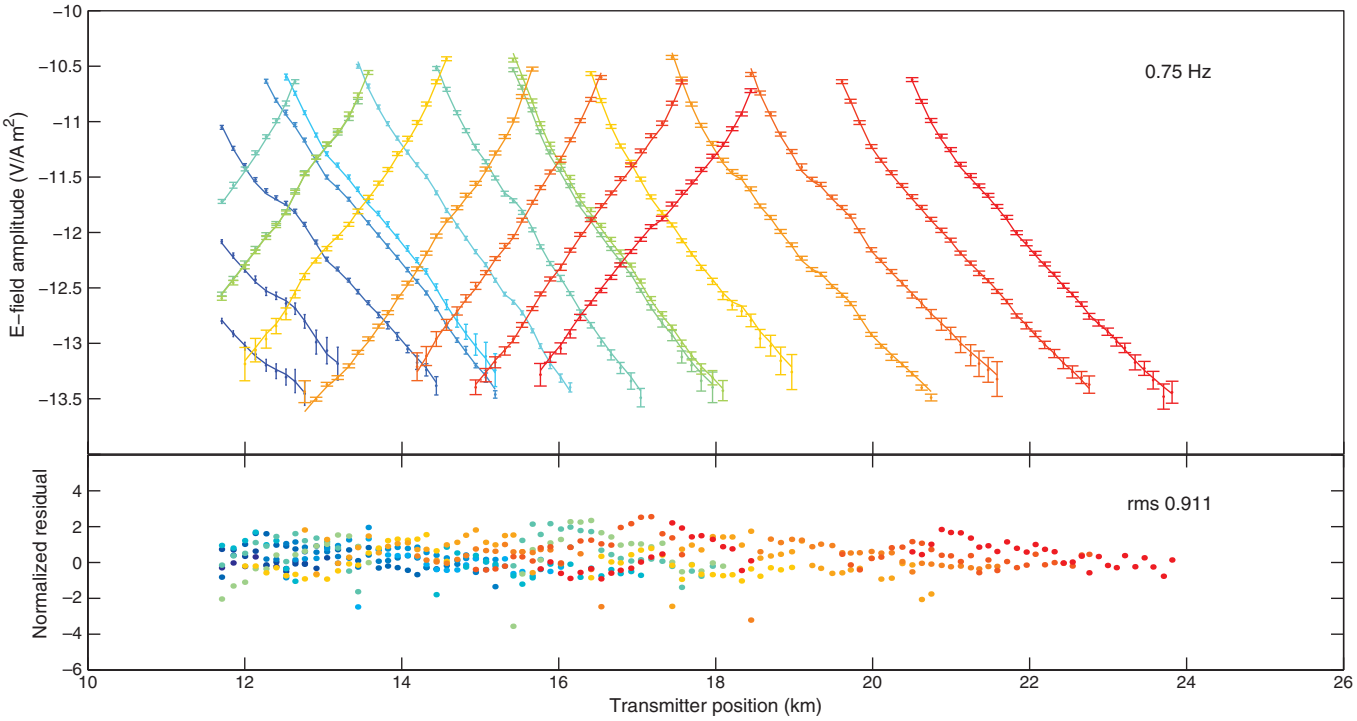

Figure 5. Marine CSEM data at the 0.75-Hz harmonic as a function of the transmitter position. The model response and normalized residuals are from an anisotropic inversion fitting the entire CSEM and MT data set to rms 0.90 and shown in Figure 12. The rms misfit for this data subset is 0.911.

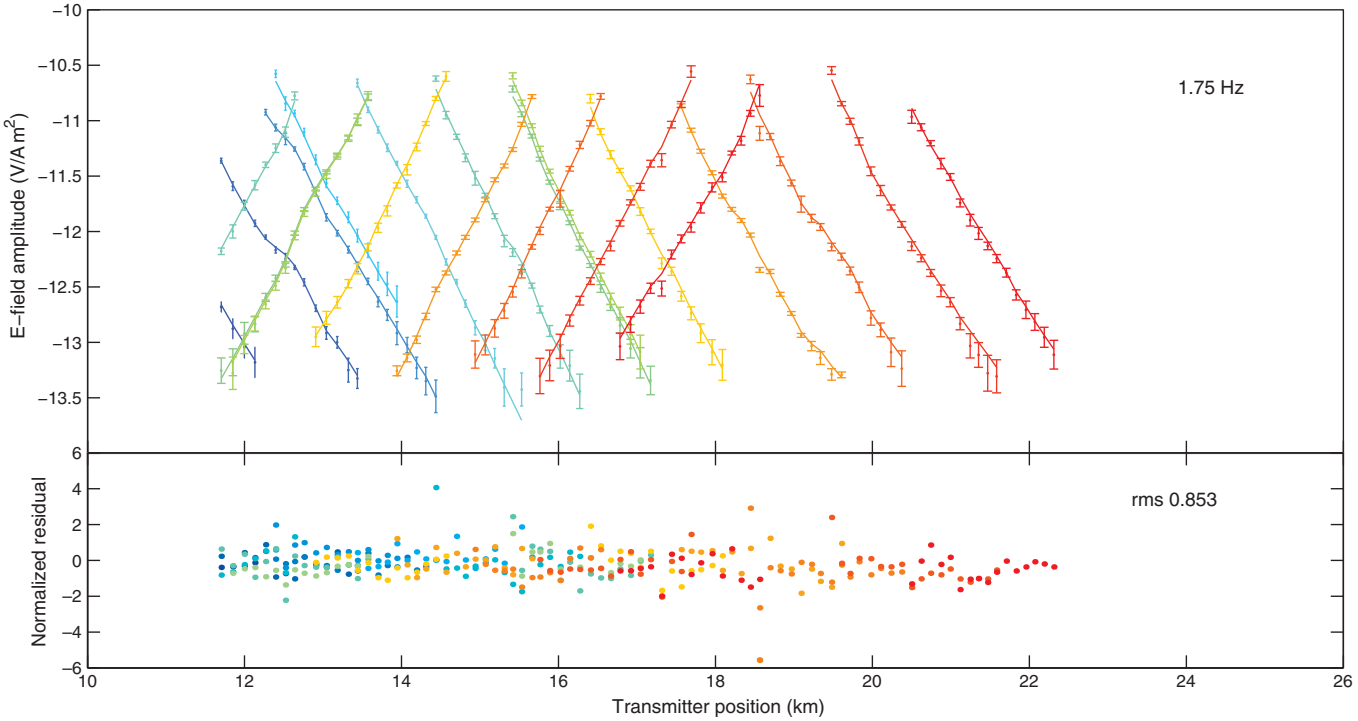

Figure 6. Marine CSEM data at the 1.75-Hz harmonic as a function of the transmitter position. The model response and normalized residuals are from an anisotropic inversion fitting the entire CSEM and MT data set to rms 1.20 and shown in Figure 12. The rms misfit for this data subset is 0.853.

space, choosing an unrealistically small target misfit. We ran each inversion until no significant improvement in misfit occurred. The resulting misfits are documented in Table 1, which also shows the starting misfit associated with the 1-Ωm half-space. Figure 7 shows CSEM single-frequency and MT models rerun to converge for misfits that are chosen to be close to the minimum achievable, to demonstrate the depth sensitivity and the kind of conductivity structures that are required to fit the data. It can be seen from the model plots that the depth of investigation of the CSEM data clearly decreases with frequency, but interestingly, the 0.75-Hz data are not as well fit as the other frequencies nor does the 0.75-Hz model exhibit as much structural complexity. On the other hand, the three CSEM frequencies are sensing similar structural patterns that are also compatible with the shallowest part of the MT model. Deeper in the section, the MT model shows the salt body between a 2- and 4-km depth and a basement at a 6-km depth. That the minimum misfits from inversions of individual data subsets are all below a normalized rms misfit of 1.0 (the expectation value) suggests that our error estimation has been reasonably successful and that the 2D approximation is adequate to fit the data. The use of an error floor introduces some subjectivity into the error estimation, but the error floors used here are based on many years of experience.

Table 1. Misfits of the various data subsets and combinations, where rms start is the starting half-space of 1 Ωm, rms min. is the best achievable misfit for inversions of the individual data subsets, and rms aniso. is the misfit of the individual data subsets for the best-fitting (rms = 0.90) joint anisotropic model shown in Figure 12.

Inversion	rms start	rms min.	rms aniso.	No. data
MT only	4.926	0.996	1.083	338
0.25-Hz CSEM	6.275	0.773	0.836	675
0.75-Hz CSEM	12.972	0.986	0.911	453
1.75-Hz CSEM	9.000	0.579	0.853	303
3-freq. CSEM	9.434	0.934	—	1431
All data	8.754	1.057	0.900	1769

ISOTROPIC JOINT CESM/MT INVERSIONS

Having demonstrated that the individual data subsets can be inverted to compatible and reasonable misfits, we combined all three

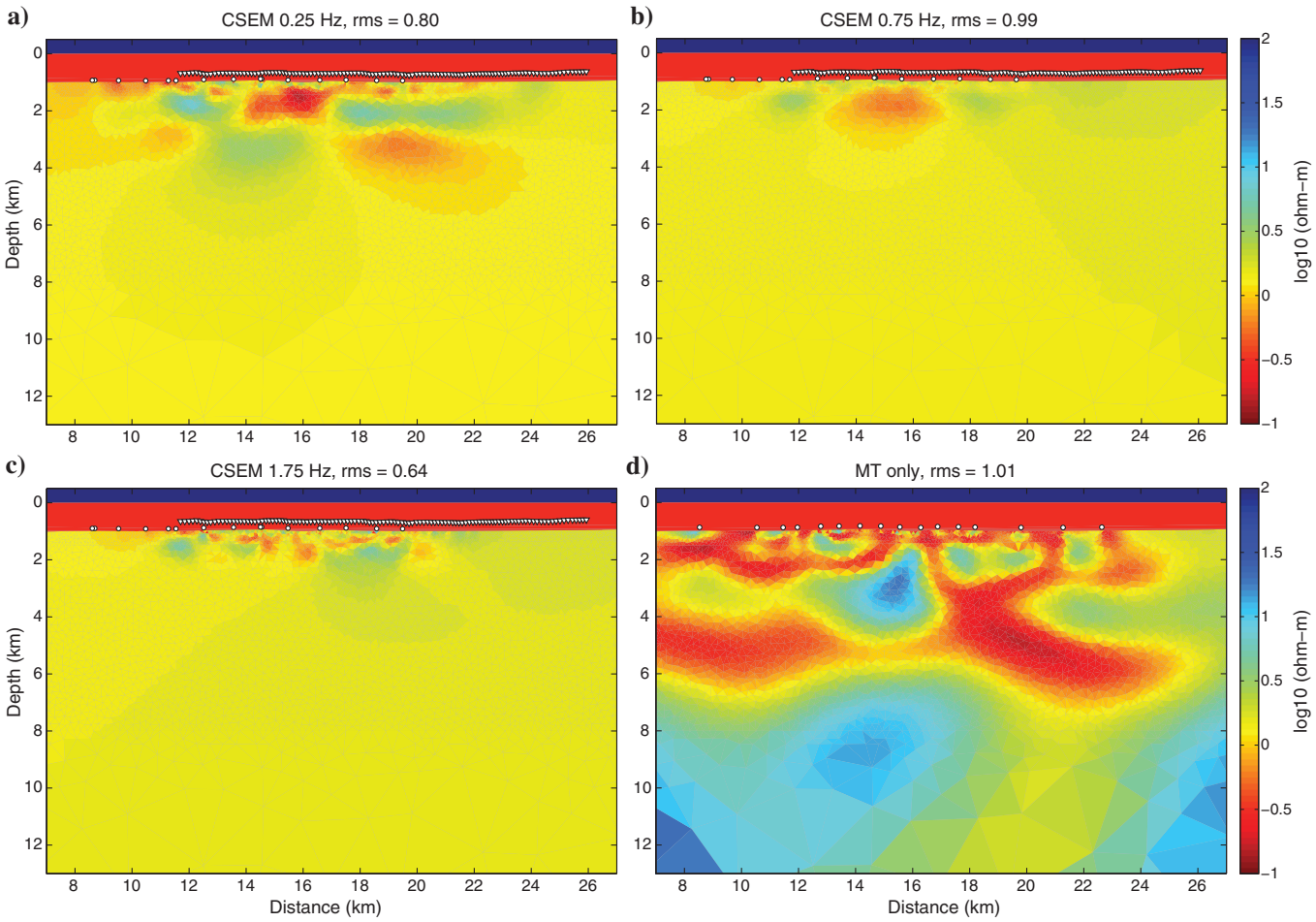

Figure 7. (a-c) Isotropic models from individual CSEM frequencies and (d) MT-only data inverted for misfits close to the minimum achievable as noted in Table 1. The locations of the receivers are shown by white circles, and the transmitter locations are white triangles.

CSEM frequencies, and we also combined MT and all CSEM data. One problem that arises when CSEM and MT data are jointly inverted is that the number of CSEM data points almost always exceeds the number of MT data points by a considerable amount (here 1431 data versus 338 data; see Table 1). Application of the standard Occam algorithm often produces a bias in the individual components of the misfit in favor of the CSEM data. For example, for an overall misfit of rms 2.0, the CSEM data fit to rms 1.65, and the MT data fit to rms 3.06 using an unmodified inversion. We address this problem by scaling the weight matrix $\mathbf{W}_i$ of the ith data subset by $\sqrt{1/n_i}$, where n_i is the number of data in the subset, thus ensuring that both data subsets are fit to approximately the desired tolerance.

We started by inverting the joint data sets to minimum misfits (given in Table 1) using isotropic models. The three-frequency CSEM model and a joint CSEM and MT model are shown in Figure 8. The minimum misfits are close to rms 1.0 for the multifrequency CSEM and the joint MT/CSEM data sets. This is barely larger than the single-component inversions, suggesting overall compatibility between all of the data components.

The effect of combining CSEM frequencies is profound (Figure 8a). The salt body, barely visible as a smudge in the 0.25-Hz inversion and completely absent from the higher frequency inversions, is now pronounced, with a well-defined top and even a reasonably defined base. The conductive region evident in the 0.25- and 0.75-Hz inversions has now developed into a narrow conductive layer draped over the salt body, suggestive of brines associated with the salt. The shallow resistive layers to the northeast and southwest of the salt, diffuse in the single-frequency inversions, are now developed as thin layers overlying the conductive feature. The resistivity of the deep section has increased from approximately 1 to 2–3 Ωm, but this is likely a result of the regularization "bleeding" the higher salt resistivity into the unresolved parts of the model. This apparent improvement in resolution is presumably a consequence of moving from the purely geometric data distribution of a single-frequency amplitude sounding to a sounding that includes parametric, or mixed frequency, information with a mixture of skin depths.

The joint inversion of all data (Figure 8b) looks at first glance to be similar to the MT-only inversion (Figure 7b), but there are significant differences. The resistivity of the salt body has increased from approximately 20 to nearly 200 Ωm, although the overall shape has remained similar. The shallow conductive and resistive layers seen in the CSEM inversion are evident, but the shallowest part of the section has broken into a confused structure of alternating conductors and resistors. This is symptomatic of incompatibilities in the data associated with MT sensitivity to horizontal conductivity and CSEM sensitivity to vertical resistivity, which we will address in the section on anisotropy below, but it may also be due to overfitting the data by requesting a misfit close to the minimum obtainable.

Interestingly, although the CSEM data clearly do not have any sensitivity below approximately a 5-km depth, there are significant changes at much deeper depths in the joint model compared with the MT-only inversion. This may be interpreted in terms of the CSEM data placing additional constraints on the near-surface structure that must be accommodated by the MT data. Changing the near-surface structure seems to have prevented the MT data from allowing the structure to leak into the basement resistor through the regularization penalty. The overall effect is that the basement resistor is now more laterally continuous, which may be regarded as a more plausible model.

Although our ability to fit the joint data sets close to rms 1.0 is consistent with our error estimates and 2D model assumption, fitting the data to the minimum possible misfit is very likely to result in a structure that had developed largely as an attempt to fit noise in the data. We therefore examined the trade-off between the data misfit and model complexity for the joint MT/CSEM data set. We started the inversion exercise by inverting the data from an isotropic half-space of 1 Ωm to a conservative misfit of rms 2.4, being sure to allow the inversion to converge to the smoothest model. The inversion was restarted from this model and allowed to converge to a target misfit of rms 1.7, then this model was restarted with a target of rms 1.3, and so on. A sample of the results is shown in Figure 9, and the individual component misfits and roughness measures are given in Table 2.

These models provide some sense of which features are required even when large amounts of data misfit are tolerated and how the model complexity increases with decreasing data misfit. The fea-

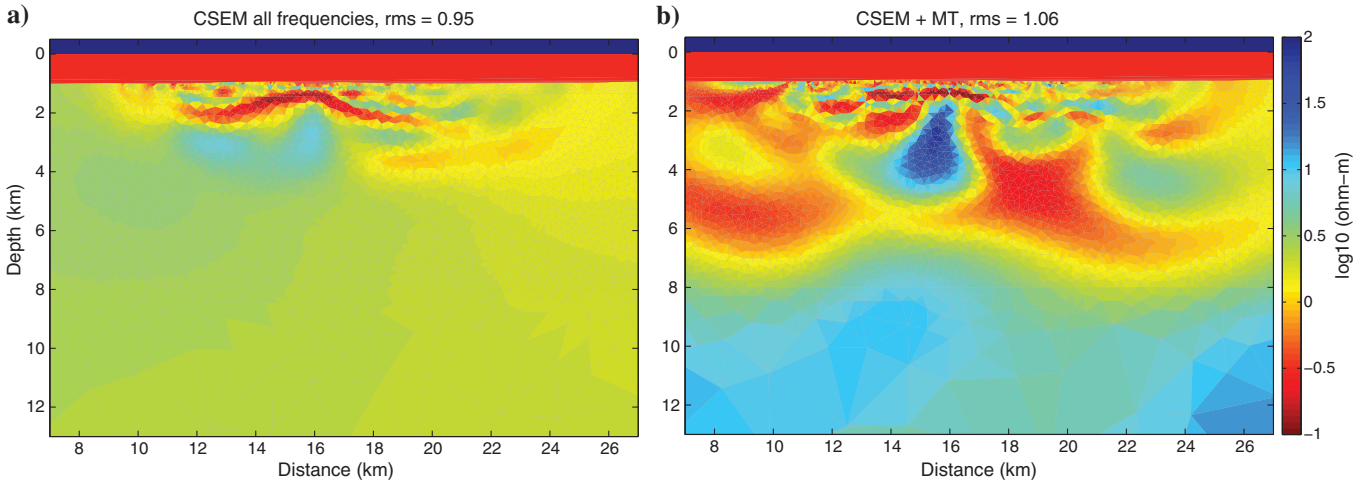

Figure 8. Isotropic models from joint inversion of (a) all CSEM frequencies and (b) all CSEM and MT data for misfits close to the minimum achievable as noted in Table 1.

tures that first appear are the basement, salt, conductor overlying the salt, and a resistive layer about 500 m below the seafloor. It is reassuring that some important aspects of geologic interpretation, such as the fact that the salt appears not to be rooted, are evident in the most conservative misfits. However, if a quantitative estimate of the depth to base of the salt or basement is to be made, a better level of data fit is required.

Decreasing the misfit increases the resistivity contrasts, making conductors more conductive and resistors more resistive, as well as causing the near-surface structures to break up into small patches of conductive and resistive material. Although it seems reasonable to assume that the smallest misfits are demanding the inclusion of a spurious structure, how one reasonably chooses a combination of misfit and model complexity is not at all clear. One approach is to relax the misfit from the expectation value of rms 1.0 to something more conservative, such as the 95% cumulative probability of the chi-squared distribution (Smith and Booker, 1988). Unfortunately, with such a large data set, the chi-squared distribution is narrowly peaked around rms 1.0, and in this case, it gives a 95% value (rms = 1.03), which is not significantly different from the expectation value.

A trade-off curve of misfit as a function of roughness is often used as a guide for choosing the optimum misfit. Lowering the misfit demands increasing amounts of model complexity, and trade-off plots usually exhibit the characteristic "L" shape from which these curves take their name. The argument is often made that the "knee" of the L-curve provides an optimal trade-off between misfit and model complexity. There is considerable mathematic literature on the subject of L-curves, but even in the simpler case of linear systems, the arguments for choosing the knee lack mathematic rigor. Thus, for example, Hansen (1992) states that "It seems intuitively clear that a good regularization parameter λ is one that corresponds to a regularized solution near the 'corner' of the L-curve because this region is a good compromise between achieving a small residual norm and keeping the solution seminorm reasonably small." Constable (1993) makes the case that there is nothing special about the knee because it moves around as you change the scaling of the axes (rms versus sum-squared misfit; linear versus logarithmic model roughness). The largest effect, however, is the range over which one computes the data, which is demonstrated in Figure 10. The knee of the curve moves from rms 1.2 to rms 1.4 to rms 2.0 as the range of models varies. By plotting the curves against χ^2 rather than the rms misfit, the range of candidate knees can be extended to rms 2.4. Clearly, these curves provide no objective way to choose the misfit, although they represent the general range of model space we are exploring; an examination of Figure 9 shows that they span models that appear underfit and too smooth to models that appear overfit and too rough.

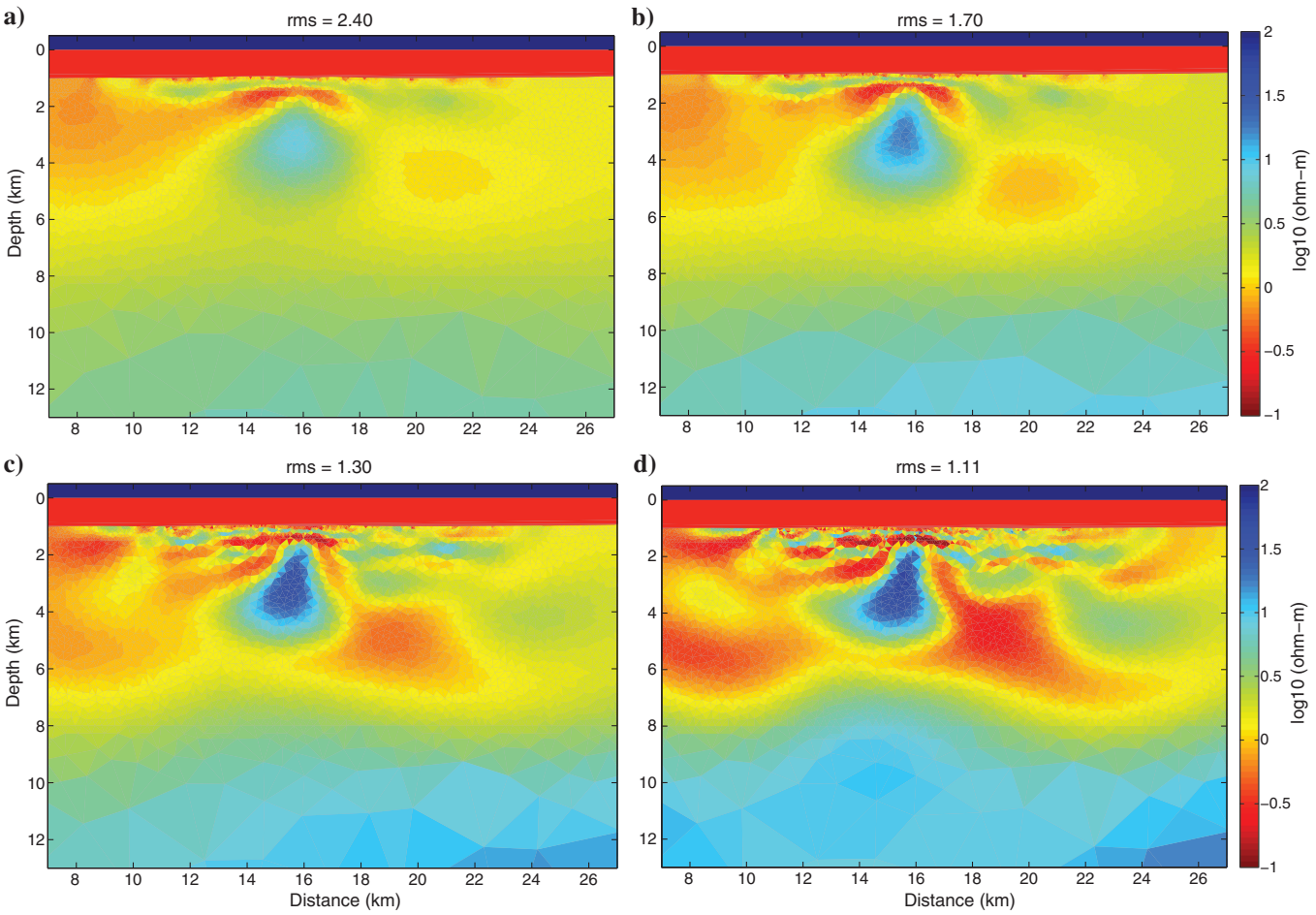

Figure 9. A sample of joint CSEM/MT isotropic inversions as a function of target misfit.

ANISOTROPIC JOINT CSEM/MT INVERSIONS

Deepwater inline CSEM data are mainly sensitive to the vertical electrical resistivity ρ_z (e.g., Constable, 2010), whereas marine MT data not strongly influenced by coastlines are mainly sensitive to horizontal conductivity σ_y. (Broadside CSEM data are also sensitive to horizontal conductivity, but such data are not available here.) Thus, if there is any anisotropy in the sedimentary section at Gemini there will be an incompatibility in the CSEM and MT data sets, similar to the incompatibility of inline and broadside CSEM modes (e.g., Lovatini et al., 2009). Constable (2010) notes that when fitting CSEM data to better than 10%–15%, the assumption that inline data are only sensitive to vertical resistivity is likely to break down, especially if using amplitude and phase at multiple frequencies. The CSEM data we are considering here may not reach this threshold of quality; even though we are inverting multiple frequencies, we do not have a phase component, and our average error is about 15%. However, the addition of MT data is causing rapid variations in near-seafloor resistivity that are symptomatic of the inversion attempting to create macroscopic anisotropy. Our next step is thus to add anisotropy to the modeling.

It is important to realize that by including anisotropy, we are doubling the number of model parameters, and unless the data can constrain the amount of anisotropy, the inversion will use this freedom to create two independent models to fit the data with minimal regularization cost. It is therefore necessary to provide some constraint on anisotropy, and one convenient way to do so is to add a regularization penalty between the vertical and horizontal resistivities. This, however, creates an additional free parameter that controls how the inversion performs, with no a priori way to choose it (essentially a second Lagrange multiplier λ in equation 2). In Figure 11, we present three anisotropic inversions with different relative weighting between the smoothness penalty and the penalty between vertical and horizontal resistivity. We choose a misfit level of rms 1.2, based on a visual assessment of the models in Figure 9 and supported by measures of randomness in the residuals presented in the next section.

Table 2. Total misfit, data subset misfits, and roughness measure (arbitrary units) for isotropic joint inversion models, four of which are shown in Figure 3.

Total misfit	CSEM misfit	MT misfit	Roughness
2.4	2.42	2.29	32.6
1.7	1.73	1.58	70.1
1.5	1.52	1.42	97.8
1.3	1.31	1.26	179
1.2	1.2	1.22	233
1.11	1.09	1.17	427
1.06	1.04	1.14	491

For a relatively weak penalty of 0.1, the vertical and horizontal resistivities are largely independent. The salt body is completely absent in the vertical resistivity (indeed, it appears as a slight conductor), which is implausible. The basement is also almost absent in ρ_z, reflecting a high degree of anisotropy, which is also unlikely, but it is understandable because the MT data have little sensitivity to vertical resistivity and the CSEM data have little sensitivity at basement depths. At the other extreme, a relative weight of 10 recovers the isotropic model with almost no discernible anisotropy, defeating the purpose of using an anisotropic inversion. A relative penalty of 1.0 produces a pleasing result, with the basement appearing as an isotropic resistor, having only a little anisotropy in the salt, and the shallow sediments appearing with a slightly higher vertical than horizontal resistivity, which is normal for horizontal bedding. Aesthetic attraction, however, represents additional input to the inversion, and the reader is reminded that because all three models fit the data equally well, the data alone provide no information on the extent of anisotropy.

As the penalty between horizontal and vertical resistivity is increased, the freedom of the models to fit the data is constrained, and the models get rougher. Thus, the models in the middle column of Figure 11, with a misfit of rms 1.2 and a penalty of 1.0, appear to have about the same level of complexity as the isotropic inversion with an rms misfit of 1.7 (Figure 9b). Put another way, allowing a modest amount of anisotropy allows the inversion to fit the data better, and in Figure 12, we explore the effect of decreasing the misfit while maintaining a relative penalty of 1.0 between the horizontal and vertical resistivities (which are parameterized as logarithms). At the cost of increased complexity, we can fit the entire data set to rms 0.9, or about 10% better than using an isotropic inversion. One should not infer from our ability to fit the data better using an anisotropic inversion that the earth is truly anisotropic; we may be using the enlarged model space to fit noise or 3D effects in the data better. For example, returning to Figure 11,

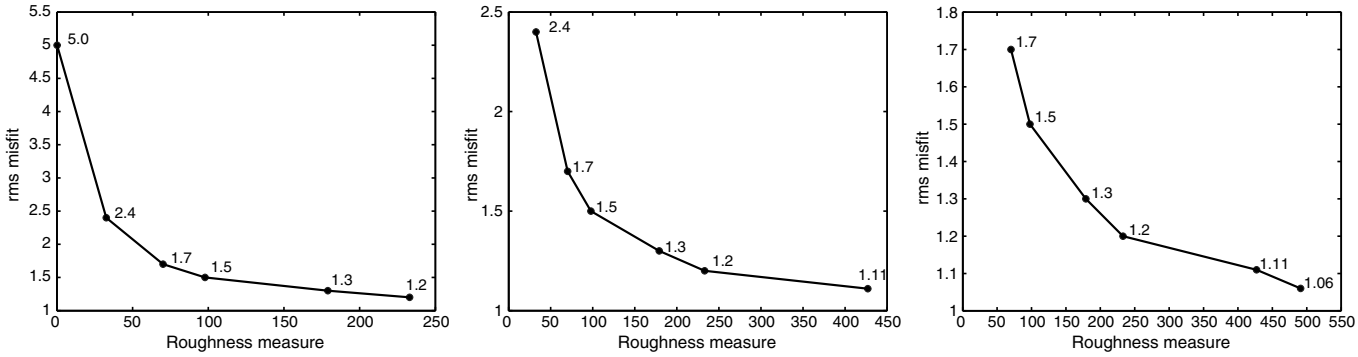

Figure 10. Plots of rms misfit versus model roughness for isotropic inversion of the combined CSEM and MT data set (L-curves). The knee of the curve is a function of the range of data plotted.

at a penalty weight of 0.1, there is significant anisotropy in the salt and basement that is not likely to be representative of the geology. We could restrict anisotropy to the sediments by using a relative penalty that increased with resistivity, but there are geologic circumstances where there will be anisotropy in the more resistive part of the section (such as interbedded volcanic flows).

STRUCTURE IN RESIDUALS

We have shown that we are able to fit our data set, separately and collectively, to about rms 1.0, the expected misfit. This is encouraging, but we should examine the structure of the residuals for any systematic effects, outliers, and bias toward one component or another. In Figure 3, we plot the MT response of the rms 0.9 joint anisotropic model, the best-fitting inversion for the combined data set. We also plot normalized residuals for amplitude and phase as a function of site. The residuals are of uniform size between sites and show no particular bias as a function of frequency. There are no egregious outliers, although the highest frequency resistivities of sites 3 and 6 produce residuals of nearly −4. Figure 13 shows histograms of normalized residuals for MT resistivity and phase. MT phase data are fit a little better than resistivity data, but not by a large amount (rms 0.98 versus rms 1.18). The MT residuals pass a Kolmogorov-Smirnov (K-S) test for normality at a significance level of 95%, collectively and separately for amplitude and phase, and the mean of the residuals is indistinguishable from zero.

In Figures 4–6, we plot normalized residuals for the CSEM data as a function of transmitter position, again for the rms 0.9 anisotropic model response. There is some serial correlation evident with a length scale of approximately 1 km and one egregious outlier in the 1.75-Hz data at a transmitter position of 18.5 km. There is some evidence that the long-range data at the end of the tow are being fit better than are shorter range data, which is consistent with errors in the transmitter and/or receiver navigation. However, the misfit is evenly distributed across the three frequencies, more so than for the inversions of individual frequency data. The histograms of the residuals, plotted in Figure 13, are visually similar to a normal distribution, but they do not pass a K-S test against a normal distribution. The residuals for the 0.25-Hz data are indistinguishable from zero-mean, but for the two higher CSEM frequencies, which

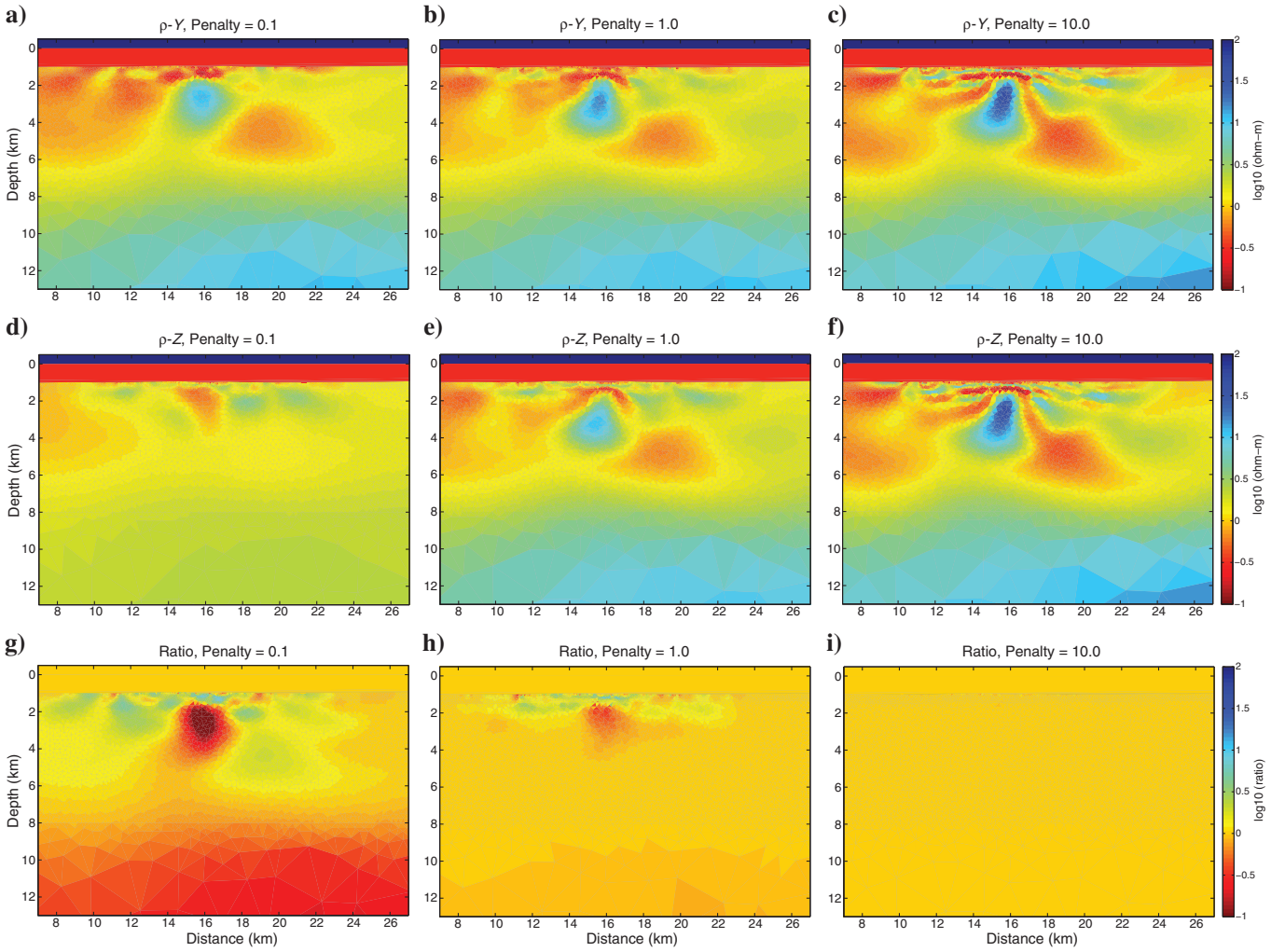

Figure 11. Joint CSEM/MT anisotropic inversions for an rms misfit of 1.2, as a function of relative penalty between ρ_z and ρ_y. Panels (a-c) show horizontal resistivity as a function of penalty, panels (d-f) show vertical resistivity, and panels (g-i) show the anisotropy ratio log (ρ_z/ρ_y).

have mean residuals of 0.3 and 0.2, respectively, the mean residuals are three or four times the error in the mean. Collectively, the combined MT and CSEM residuals have a mean indistinguishable from zero, but they do not pass a K-S test.

Our ability to fit the combined CSEM/MT data set to a little better than rms 1.0, with residuals that are largely normal, evenly distributed across the data, and zero mean might suggest that the rms 1.0 anisotropic inversion in Figure 12 is optimal. Certainly, it implies that we have done a reasonable job of error estimation, but a 10% increase or decrease in the overall error size would allow us to declare any of the models in Figure 12 as optimal. Furthermore, it is essentially impossible to quantify how well the 2D geometry approximates the real geology. We are, again, reduced to subjective decisions about what represents a reasonable amount of model complexity.

It is very convenient to measure the quality of models using a global measure such as the rms misfit. Indeed, the sum-squared misfit is essential to the optimization machinery we use to construct the models. However, besides assuming that the data errors are normally distributed and zero mean, our starting assumptions included independence between data errors. That is, the residuals should appear random, particularly as a function of position (for CSEM data) or period (for MT data). Figure 14 shows residuals for the best-fitting isotropic model (rms = 1.06) as a function of CSEM source-receiver range and MT period, and a similar plot for a poorly fitting model (rms = 2.40). Apart from increased scatter, the poorly fitting model has a lot of structure in the residual plots, with evident serial correlation in the residuals as a function of range or period. This suggests that we should search for some measure of this serial correlation that might provide an indication of when an adequate fit to the data has been achieved.

One good statistical test for serial correlation or randomness is the one-sample runs test (e.g., Crow et al., 1960). This test examines the sign of the residuals as a function of the source-receiver offset or period: Many consecutive residuals with the same sign indicate nonrandomness or serial correlation. In Figure 15, we plot the fraction of data subsets (in red) that pass the runs test at the 95% confidence level as a function of misfit. (The total number of data subsets is 74, and the data in Figure 15 come from isotropic fits with the exception of the rms = 0.9 data point, which is from an anisotropic inversion.) Unfortunately, about a quarter of the data subsets of even the best-fitting anisotropic model fail the runs test because there is a residual structure within the residuals, especially the CSEM data. There is not a particularly large change in the fraction of subsets that fail the runs test as we improve the misfit.

A related statistic is the probability that the entire data set is not random, again using the runs test (Figure 15, green line). Again, even the best-fitting model has only a 50% chance of having random residuals, and there is not much structure to the curve as a function of misfit, although there is a small change of slope at around rms = 1.2.

One of the statistical assumptions is that the error process is zero mean. In blue, we plot the mean of the residuals (scaled by two to fit better in the figure), and here we do see a significant improvement as a function of decreasing misfit, with the mean residual decreasing from about 2.3 to 1.2. However, the curve is close to a straight line, providing little guidance as to when we may be reaching a critical threshold in the structure of the residuals.

Similarly, the average slope of least-squares line fits to the data residual subsets (shown as black lines in Figure 14) normalized by the error in the slope's estimation shows a monotonic improvement with improving misfit, with no obvious break point (Figure 15, light blue). However, taking an approach similar to that of Constable and Cox (1996), if we consider the number of data subsets for which the least-squares slope exceeds the error in the slope (the black line in Figure 15, scaled by 10 to fit the figure), we see that the number of

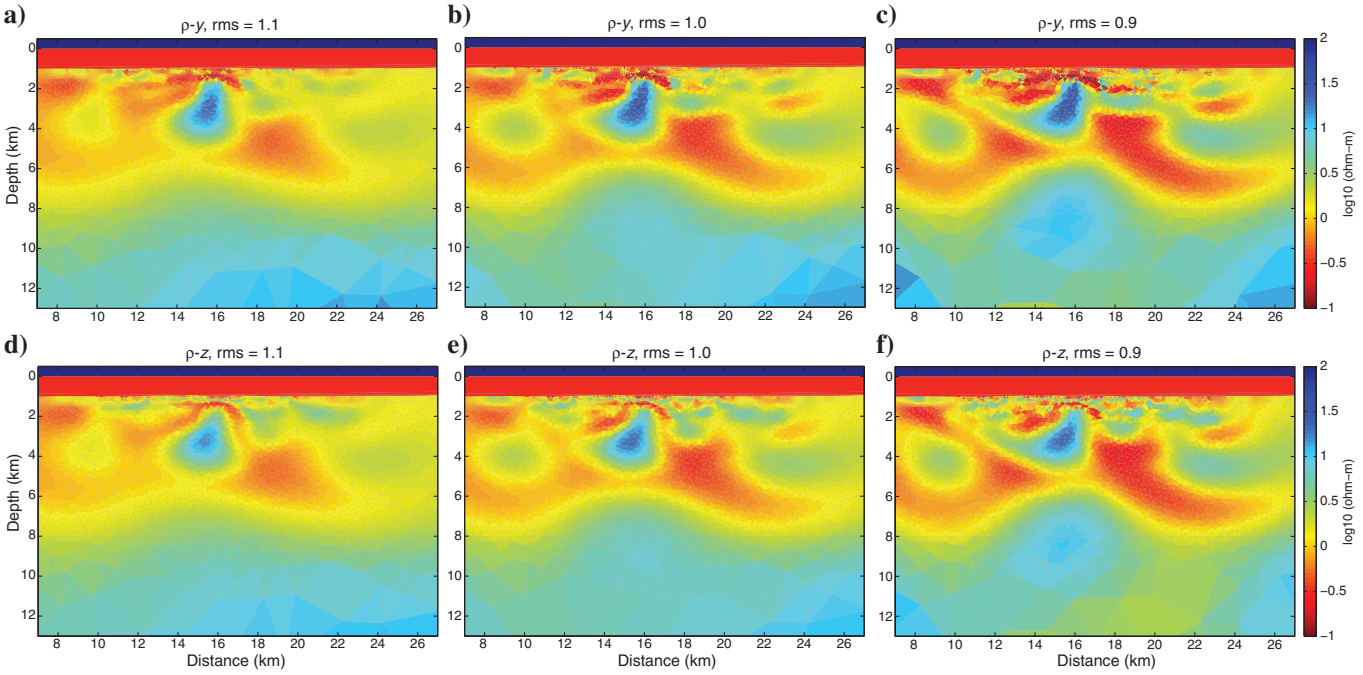

Figure 12. Joint CSEM/MT anisotropic inversions for rms misfits of 0.9, 1.0, and 1.1, all with a relative penalty between ρ_z and ρ_y of 1.0. Panels (a-c) show horizontal resistivity as a function of misfit, and panels (d-f) show vertical resistivity.

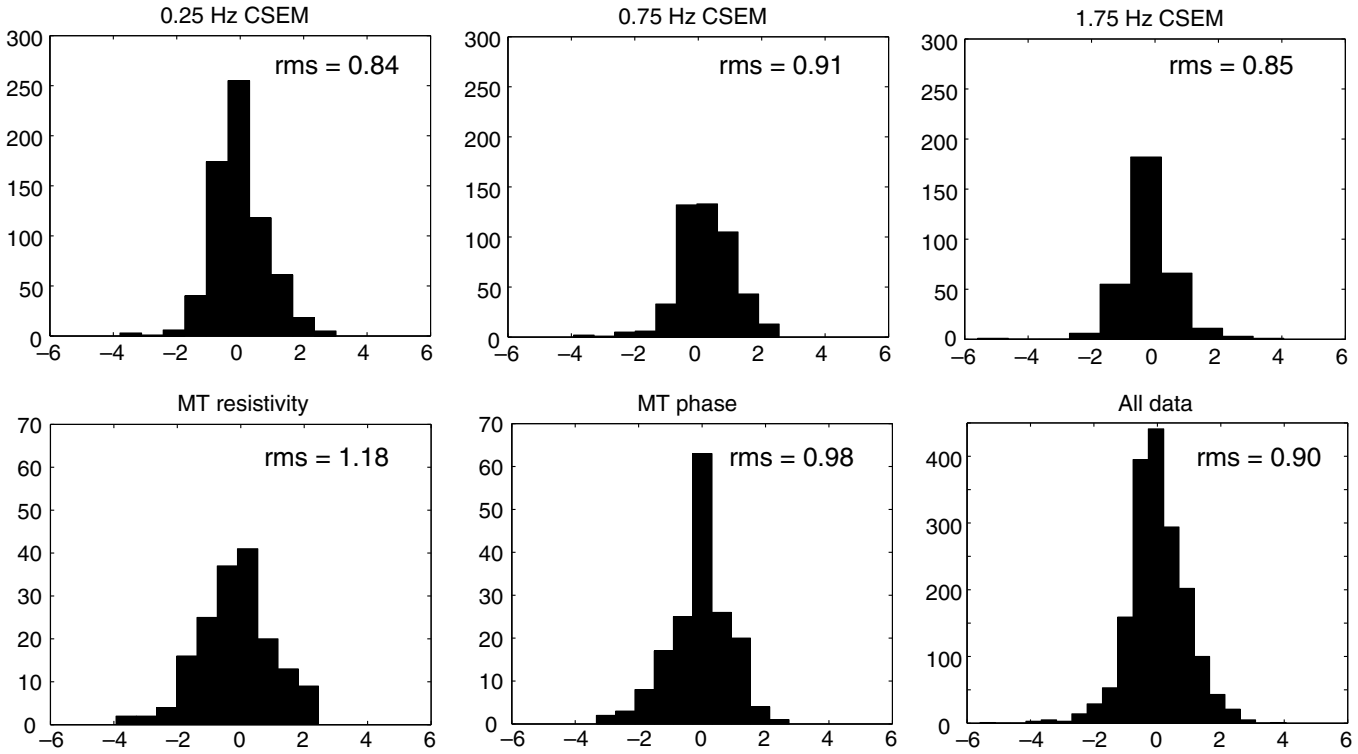

Figure 13. Histograms of normalized residuals for all data subsets from an anisotropic inversion fitting the entire CSEM and MT data set to rms 0.90 and shown in Figure 12.

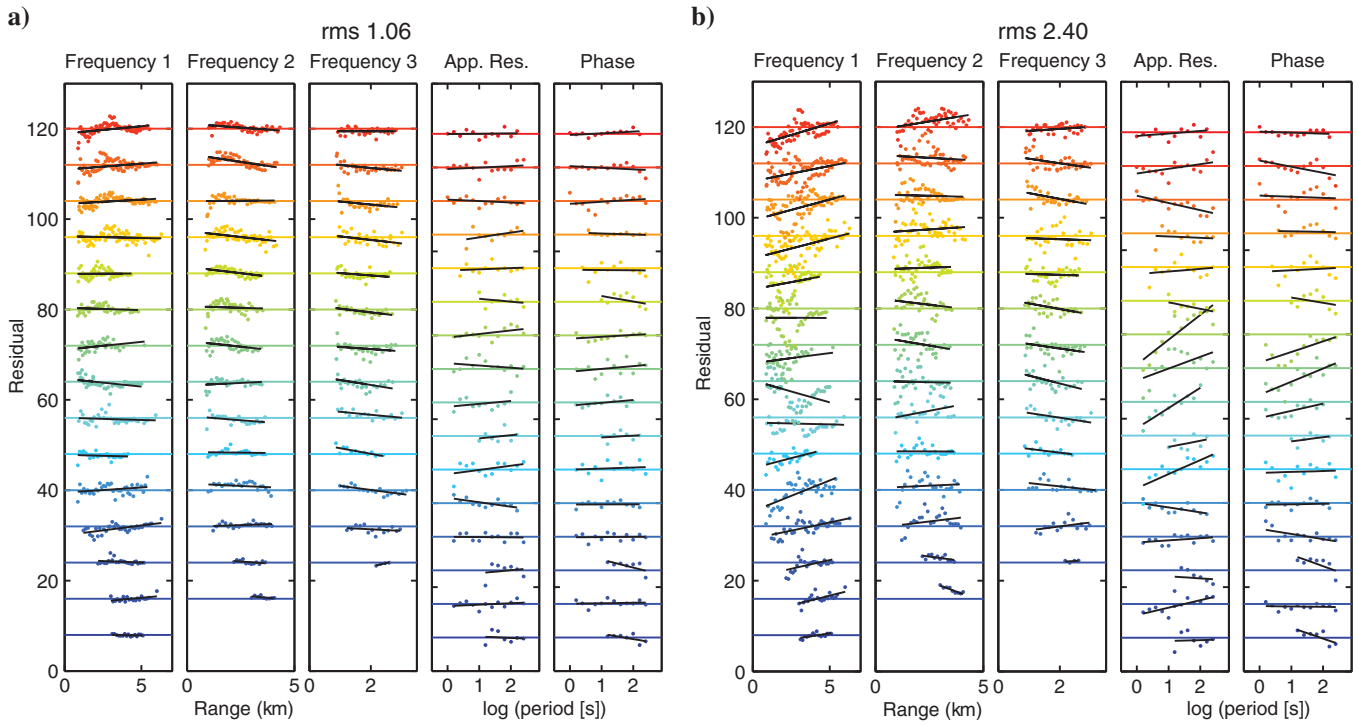

Figure 14. (a) Residuals for an isotropic rms = 1.06 model, plotted by site (distinguished by color) and by CSEM source-receiver range or MT period (horizontal axis). Sites have been plotted with a vertical offset to separate them, with zero shown by the colored horizontal lines. The black lines are least-squares linear fits to the residuals. (b) As for (a), but for the poorly fitting rms = 2.40 model.

data subsets falls from 14 to four, with a rapid decrease at rms = 1.2 followed by no change with a lower misfit. Entirely heuristically, this may be an indication that at around rms = 1.2, we obtain a sudden decrease in the structure of residuals with little improvement after that.

WHAT IS TRUTH?

The purpose of this paper is not to discuss Gulf of Mexico geology, but it is useful to compare the EM inversion models with what is known about structure in the Gemini area to obtain some idea of what might be an inversion artifact and what might be driven by a real structure. In Figure 16, we overlay seismic reflectivity on the rms = 1.0 joint MT/CSEM anisotropic model to look for structure that correlates between the two (very different) geophysical methods. As Key et al. (2006) observe from MT-only inversions, the shallow, thick part of the salt body is fairly well resolved. The separation between the salt and basement structure is better than for the MT-only inversion. Interestingly, it is only the joint anisotropic inversions that place a resistor at the deeper, thinner salt to the southwest: The isotropic inversions presented here place this resistor above the salt, which is too shallow in the section. The pronounced conductor draped over the salt is not evident in the MT-only inversions, in spite of the conventional wisdom that MT is preferentially sensitive to conductors, and this suggests that brines have accumulated above the shallower parts of the salt body. This is evident in the well logs. Figure 17 shows the well log from OCS-G-8806, redrawn by hand from a scanned version of the 14-m-long original hardcopy provided by the Bureau of Ocean Energy Management. A 400–500-m-thick layer of 0.3 Ωm sediment immediately overlies the salt body, in fairly good agreement with the inversions. Although the log is saturated over much of the salt section, the salt appears to be around 20 Ωm or more, again in agreement with the inversions.

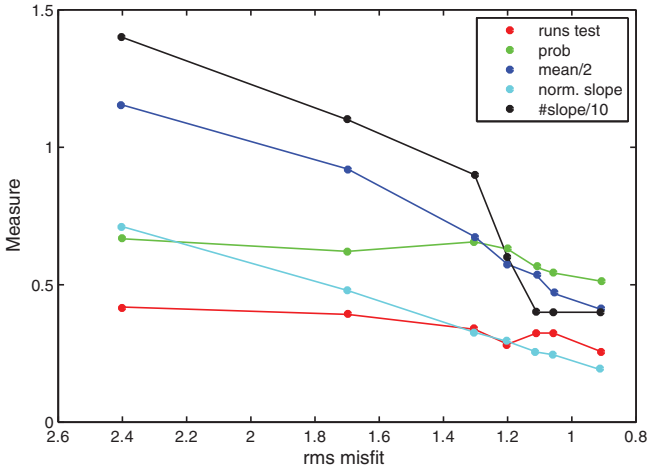

Figure 15. Various tests of structure in the data residuals binned by data subset as illustrated in Figure 14: red, the fraction of subsets that pass a runs test; green, probability that the ensemble of data subsets is nonrandom based on the runs test; dark blue, the mean of the residuals (divided by two for plotting); light blue, average absolute value of the slopes of least-squares line fits to data subsets, normalized by standard error in the slopes; black, number of data subsets in which the slope divided by its standard error is greater than 1.0 (divided by 10 for plotting).

DISCUSSION

On the order of 100 inversions were carried out as part of this study. Early inversions were used to define the minimum source-receiver ranges at which the CSEM data were unaffected by navigation errors and amplifier saturation (we were still using amplifier gains of 10^6 when these data were collected), as well as allow us to refine the forward model dimensions and parameterization. Many inversions explored aspects of model complexity versus misfit beyond the representative examples presented in this paper. To illustrate how regularized inversion depends on misfit, data type, model parameterization, and regularization parameters, we have run a broader range of inversions than would normally be examined during "routine" inversion of a geophysical data set. However, we use the results shown here to make the case that to fully understand a geophysical data set and derive a meaningful model using inver-

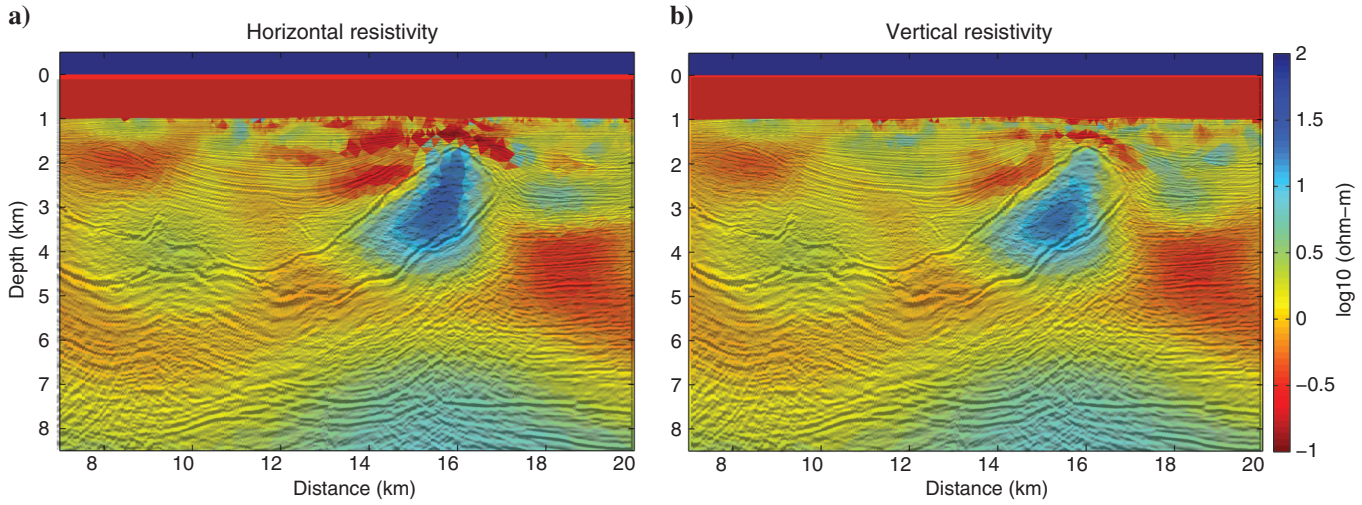

Figure 16. Overlay of seismic reflectivity (courtesy of Chevron) on rms 1.0 anisotropic inversions of joint MT/CSEM data set: (a) horizontal resistivity and (b) vertical resistivity.

sion algorithms, many inversions need to be run. We have generated dozens of models, all different, that, based on misfit, could reasonably be considered compatible with the data we have collected, and even so, we have used only one type of inversion algorithm. Other algorithms and regularization schemes will produce a different suite of models.

The computational cost of current 3D inversion technology would make such an extensive exploration of model and misfit space expensive, perhaps prohibitively so, although we certainly expect that in the future this will improve. The danger associated with running a single, or a small number, of inversions is that the resulting structures might be considered representative of the real earth, when in fact they may be more representative of model parameterization, data error structure, or some other characteristic. One-dimensional inversion is extremely rapid, but it does not address issues of site-to-site consistency of data structure and error structure. We suggest that 2D inversion provides an effective way to explore an EM data set before the computational cost of 3D inversion is expended.

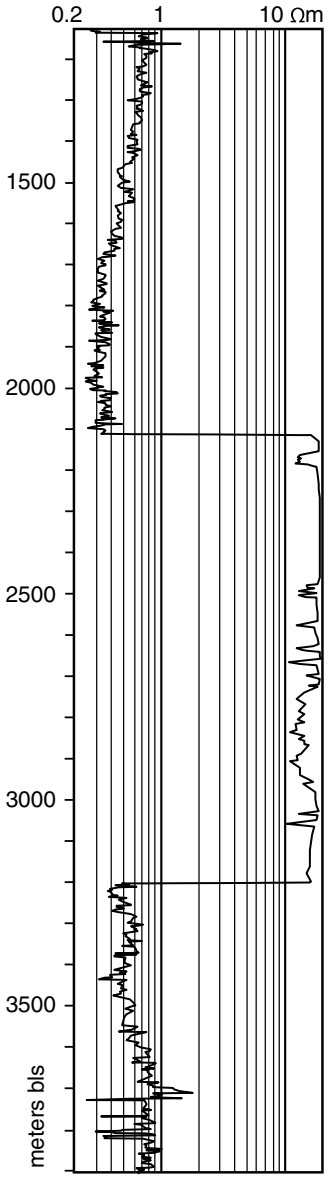

Figure 17. Well log from well OCS-G-8806 number three, redrawn by hand.

Our study has demonstrated the value of inverting multicomponent EM data, in particular multiple frequencies of CSEM data. It is easy to think of marine CSEM sounding as dominated by geometric parameters, given its resemblance to dipole-dipole resistivity and the relationship between the source-receiver offset and target depth, but clearly, the role of skin depth is important. The value of using multiple frequencies has already been demonstrated for 1D inversion (Key, 2009), but the effects in 1D are modest compared with what we observe in the 2D inversions presented here. Unfortunately, the vintage of the data used in this study did not allow us to examine the role of the CSEM phase, but we note that this amplitude-only data set is representative of many early commercial data sets.

The value of joint MT and CSEM inversion has long been recognized, since at least the 1970s (Vozoff and Jupp, 1975). One challenge to the use of combined MT and CSEM data in the marine environment is creating an overlap in the depth sensitivity of the methods. This is maximized by increasing the frequency of the MT responses in spite of the red spectrum of source-field energy and the attenuating effects of seawater and increasing the source-receiver offsets of the CSEM data. However, one of the interesting results of our study is that by providing constraints on the near-surface conductivity structure from CSEM data, the deeper structure sensed by the MT data is modified over MT-only inversions in ways that subjectively appear to be improvements (higher resistivity in the salt body and more uniform resistivity in the basement).

Although we emphasize the value of careful error estimation, the use of objective statistical guides to choose optimal misfit levels (expectation value, 95% confidence levels, etc.) requires an accuracy of error estimation and fidelity of the model approximations that are rarely, if ever, achieved in practice, and this study is no exception. Although errors are often close to Gaussian, they almost always lack independence as a result of systemic effects in the data collection and processing. This distinguishes real-world data interpretation from synthetic model studies. We have shown that the so-called L-curves can be heavily biased by plotting parameters and are of little use. However, structure in the residuals as a function of the CSEM source-receiver offset or MT frequency can be used as a guide to an adequate fit, and in particular, a significant slope to the residuals may pass through a threshold associated with diminishing returns in the roughness-misfit trade-off. But, like the L-curve knee, this is somewhat heuristic.

CONCLUSIONS

There exists an old joke: The exploration manager asks a geologist, engineer, and a geophysicist what $2 + 2$ is. The geologist replied "somewhere between 3 and 5," the engineer replied "about 3.99," and the geophysicist replied "what answer do you want?". The joke is somewhat cruel to all three disciplines, but it does highlight the problem of nonuniqueness in geophysical inversion. However, a thorough exploration of model space, along with careful choice of data error structure and examination of misfit residuals can help the interpreter understand which features of the models are reliable and which are potentially a result of overfitting the data. Introduction of geologic information, other data constraints, and common sense is an important part of geophysical interpretation.

For example, it was surprising to see how poorly anisotropy was constrained by our data set, but the introduction of sensible limits on anisotropy based on geologic principles would quickly eliminate the extremal models. It is likely that the inclusion of 3D CSEM data would also constrain anisotropy better than the 2D example presented here, but a careful exploration of model space would still be warranted. In conclusion, it is not one model that you want, but many.

ACKNOWLEDGMENTS

The authors thank J. Behrens, M. Everett, R. Reddig, and C. Weiss for participating in the data-collection cruise, J. Behrens for initial processing of the CSEM data set, and D. Bartel and Chevron for making the seismic images and salt volumes available. S. Constable and K. Key collected the data, and A. Orange ran the inversions and contributed to the interpretations. The computer code was written by K. Key and S. Constable. S. Constable wrote the initial draft of the manuscript with input from A. Orange and K. Key. Careful reviews by R. Mittet, M. Zhdanov, and an anonymous reviewer are appreciated, and they led to significant improvements in the manuscript. This work was supported by the Seafloor Electromagnetic Methods Consortium at Scripps Institution of Oceanography, with additional support for the CSEM data collection provided by ExxonMobil Upstream Research Corporation.

REFERENCES

Commer, M., and G. A. Newman, 2008, New advances in three-dimensional controlled-source electromagnetic inversion: Geophysical Journal International, **172**, 513–535, doi: 10.1111/j.1365-246X.2007.03663.x.

Commer, M., and G. A. Newman, 2009, Three-dimensional controlled-source electromagnetic and magnetotelluric joint inversion: Geophysical Journal International, **178**, 1305–1316, doi: 10.1111/j.1365-246X.2009.04216.x.

Constable, S. C., 1993, Constraints on mantle electrical conductivity from field and laboratory measurements: Journal of Geomagnetism and Geoelectricity, **45**, 707–728, doi: 10.5636/jgg.45.707.

Constable, S., 2010, Ten years of marine CSEM for hydrocarbon exploration: Geophysics, **75**, no. 5, 75A67–75A81, doi: 10.1190/1.3483451.

Constable, S., 2013, Review paper: Instrumentation for marine magnetotelluric and controlled source electromagnetic sounding: Geophysical Prospecting, **61**, 505–532, doi: 10.1111/j.1365-2478.2012.01117.x.

Constable, S., and C. S. Cox, 1996, Marine controlled source electromagnetic sounding 2. The PEGASUS experiment: Journal of Geophysical Research, **101**, 5519–5530, doi: 10.1029/95JB03738.

Constable, S., A. Orange, G. M. Hoversten, and H. F. Morrison, 1998, Marine magnetotellurics for petroleum exploration: Part 1 — A seafloor instrument system: Geophysics, **63**, 816–825, doi: 10.1190/1.1444393.

Constable, S. C., R. L. Parker, and C. G. Constable, 1987, Occam's inversion: A practical algorithm for generating smooth models from EM sounding data: Geophysics, **52**, 289–300, doi: 10.1190/1.1442303.

Crow, E. L., F. A. Davis, and M. W. Maxfield, 1960, Statistics manual: Dover.

Egbert, G. D., 1997, Robust multiple-station magnetotelluric data processing: Geophysical Journal International, **130**, 475–496, doi: 10.1111/j.1365-246X.1997.tb05663.x.

Hansen, P. C., 1992, Analysis of discrete ill-posed problems by means of the L-curve: SIAM Review, **34**, 561–580, doi: 10.1137/1034115.

Key, K., 2009, 1D inversion of multicomponent, multifrequency marine CSEM data: Methodology and synthetic studies for resolving thin resistive layers Geophysics, **74**, no. 2, F9–F20, doi: 10.1190/1.3058434.

Key, K., 2012a, Marine electromagnetic studies of seafloor resources and tectonics: Surveys in Geophysics, **33**, 135–167, doi: 10.1007/s10712-011-9139-x.

Key, K., 2012b, Marine EM inversion using unstructured grids: A 2D parallel adaptive finite element algorithm: 82nd Annual International Meeting, SEG, Expanded Abstracts, doi: 10.1190/segam2012-1294.1.

Key, K. W., S. C. Constable, and C. J. Weiss, 2006, Mapping 3D salt using 2D marine MT: Case study from Gemini Prospect, Gulf of Mexico: Geophysics, **71**, no. 1, B17–B27, doi: 10.1190/1.2168007.

Lovatini, A., M. D. Watts, K. E. Umbach, A. Ferster, S. Patmore, and J. Stilling, 2009, Application of 3D anisotropic CSEM inversion offshore west of Greenland: 79th Annual International Meeting, SEG, Expanded Abstracts, 830–834.

Myer, D., S. Constable, and K. Key, 2011, Broad-band waveforms and robust processing for marine CSEM surveys: Geophysical Journal International, **184**, 689–698, doi: 10.1111/j.1365-246X.2010.04887.x.

Newman, G. A., and D. L. Alumbaugh, 1997, Three-dimensional massively parallel electromagnetic inversion. I — Theory: Geophysical Journal International, **128**, 345–354, doi: 10.1111/j.1365-246X.1997.tb01559.x.

Selway, K., 2014, On the causes of electrical conductivity anomalies in tectonically stable lithosphere: Surveys in Geophysics, **35**, 219–257, doi: 10.1007/s10712-013-9235-1.

Sherman, J., S. Constable, and R. L. Parker, 2013, Understanding noise in marine magnetotelluric measurements: Presented at AGU Fall Meeting, NS31A-1668.

Smith, J. T., and J. R. Booker, 1988, Magnetotelluric inversion for minimum structure: Geophysics, **53**, 1565–1576, doi: 10.1190/1.1442438.

Smith, R., 2014, Electromagnetic induction methods in mining geophysics from 2008 to 2012: Surveys in Geophysics, **35**, 123–156, doi: 10.1007/s10712-013-9227-1.

Tikhonov, A. N., and V. Y. Arsenin, 1977, Solutions of ill-posed problems: Winston.

Vozoff, K., and D. L. B. Jupp, 1975, Joint inversion of geophysical data: Geophysical Journal of the Royal Astronomical Society, **42**, 977–991, doi: 10.1111/j.1365-246X.1975.tb06462.x.

Zhdanov, M. S., S. Fang, and G. Hursán, 2000, Electromagnetic inversion using the quasilinear approximation: Geophysics, **65**, 1501–1513, doi: 10.1190/1.1444839.

Zhdanov, M. S., L. Wan, A. Gribenko, M. Cuma, K. Key, and S. Constable, 2011, Large-scale 3D inversion of marine magnetotelluric data: Case study from the Gemini prospect, Gulf of Mexico: Geophysics, **76**, no. 1, F77–F87, doi: 10.1190/1.3526299.